Electrochemical performance of $Na_2Ti_3O_7$/C negative electrode in ionic liquid electrolyte for sodium secondary batteries

Changsheng Ding[a], Toshiyuki Nohira[b,*] and Rika Hagiwara[a,*]

[a] Graduate School of Energy Science, Kyoto University, Sakyo-ku, Kyoto 606-8501, Japan
[b] Institute of Advanced Energy, Kyoto University, Uji 611-0011, Japan

* Corresponding authors. Tel.: +81 75 753 5822; fax: +81 75 753 5906.
E-mail addresses: nohira.toshiyuki.8r@kyoto-u.ac.jp
hagiwara@energy.kyoto-u.ac.jp

Abstract

In this study, carbon-coated $Na_2Ti_3O_7$ ($Na_2Ti_3O_7$/C) is synthesized by a solid-state reaction method, and its charge-discharge characteristics as a negative electrode material in an ionic liquid electrolyte, Na[FSA]-[C_3C_1pyrr][FSA] (FSA = bis(fluorosulfonyl)amide; C_3C_1pyrr = *N*-methyl-*N*-propylpyrrolidinium), are investigated at 363 K. The $Na_2Ti_3O_7$/C negative electrode shows an initial discharge capacity of 215 mAh (g-$Na_2Ti_3O_7$/C)$^{-1}$ at a current rate of 20 mA (g-$Na_2Ti_3O_7$/C)$^{-1}$ in the voltage range 0.01–2.5 V. The high discharge capacity of the $Na_2Ti_3O_7$/C negative electrode is attributed to the high operation temperature in the Na[FSA]-[C_3C_1pyrr][FSA] ionic liquid electrolyte. Although high discharge capacity is achieved, the $Na_2Ti_3O_7$/C negative electrode shows relatively poor cycle performance because of the irreversible insertion of some Na ions and the formation of cracks.

Keywords: Sodium secondary battery; Negative electrode; $Na_2Ti_3O_7$/C; Ionic liquid electrolyte; Charge-discharge characteristics

1. Introduction

Lithium ion batteries have received much attention as rechargeable power sources for portable electronic devices. However, some disadvantages of lithium, such as high cost, limited abundance, non-uniform distribution, and supply instability, hinder the large-scale applications of lithium ion batteries. In recent times, sodium secondary batteries are being considered as an alternative for lithium ion batteries, because of their low cost as well as sodium abundance [1-5]. Up to now, many positive electrode materials with high electrochemical performance have been developed for sodium secondary batteries [3, 6-9]. However, only a few materials have been reported as the negative electrode for sodium secondary batteries. Tin and tin alloys displayed high reversible capacities, but the large volume changes that occurred during the charge-discharge process resulted in low cycling performances [10-12]. Hard carbons showed relatively high reversible capacities of 220–315 mAh g^{-1} [13-15]. Several kinds of TiO_2 were also reported as negative electrode materials and showed reversible capacities of 80–200 mAh g^{-1} [16-18]. Recently, $Na_2Ti_3O_7$ was investigated as an alternative negative electrode material, and showed reversible capacities of 177–205 mAh g^{-1} [19-24]. Sodium ions can be reversibly inserted/extracted into/from the $Na_2Ti_3O_7$ electrode at a voltage plateau of ~0.3 V, which makes it a suitable negative electrode material.

However, the studies on $Na_2Ti_3O_7$ electrodes are usually conducted in organic electrolytes such as $NaClO_4$/propylene carbonate. Organic electrolytes are volatile and flammable, and are unsuitable as electrolytes for constructing large-scale sodium secondary batteries due to safety issues. Ionic liquids are non-flammable and have negligibly low volatility, and are thus very

suitable as electrolytes for safe large-scale batteries. We have investigated Na[TFSA]-Cs[TFSA] (TFSA = bis(trifluoromethylsulfonyl)amide) [25], NaFSA-KFSA (FSA = bis(fluorosulfonyl)amide) [26, 27], Na[FSA]-[C_3C_1pyrr][FSA] (C_3C_1pyrr = *N*-methyl-*N*-propylpyrrolidinium) [28-30] ionic liquids with $NaCrO_2$ positive electrodes and Sn, TiO_2/C, hard-carbon negative electrodes. Wang et al. [31] reported [C_4C_1pyrr][TFSA] (C_4C_1pyrr = *N*-butyl-*N*-methylpyrrolidinium) ionic liquids containing $NaBF_4$, $NaClO_4$, Na[TFSA] or $NaPF_6$ with $Na_{0.44}MnO_2$ positive electrode. Wongittharom et al. [32] studied [C_4C_1pyrr][TFSA] ionic liquids with $NaBF_4$, $NaClO_4$, $NaPF_6$ or $NaN(CN)_2$ solutes for $NaFePO_4$ positive electrode. Wang et al. [33] investigated Na[FSA]-[C_3C_1pyrr][FSA] ionic liquid with $Na_{0.44}MnO_2$ positive electrode and hard-carbon negative electrode. Hasa et al. [34] reported Na[TFSA]-[C_4C_1pyrr][TFSA] ionic liquid with P2-$Na_{0.6}Ni_{0.22}Fe_{0.11}Mn_{0.66}O_2$ positive electrode and nanostructured Sb-C negative electrode. The batteries using Na[FSA]-[C_3C_1pyrr][FSA] ionic liquid as electrolyte can be operated in a wide temperature range and show good electrochemical characteristics [28, 35, 36]. Therefore, Na[FSA]-[C_3C_1pyrr][FSA] ionic liquid was adopted as the electrolyte.

In this work, carbon-coated $Na_2Ti_3O_7$ ($Na_2Ti_3O_7$/C) powders were synthesized by a solid-state approach, and the charge-discharge characteristics of the $Na_2Ti_3O_7$/C negative electrode in Na[FSA]-[C_3C_1pyrr][FSA] ionic liquid were investigated at 363 K for the first time.

2. Experimental section

Na_2CO_3 (Sigma-Aldrich, 99.95%) and anatase TiO_2 (Sigma-Aldrich, 99.8%) powders were used as raw materials, and sucrose (Sigma-Aldrich, 99.5%) was used as a carbon source to synthesize the carbon-coated $Na_2Ti_3O_7$ powders. Firstly, the Na_2CO_3 and anatase TiO_2 powders were mixed uniformly in stoichiometric proportions and calcined in air at 1173 K for 40 h to obtain the $Na_2Ti_3O_7$ powders. The $Na_2Ti_3O_7$ powders were then mixed with sucrose, and the mixture was calcined in Ar flow at 973 K for 5 h to obtain the $Na_2Ti_3O_7$/C powders.

The crystalline phase of the synthesized $Na_2Ti_3O_7$/C powders was characterized by powder X-ray diffraction (XRD, Rigaku, SmartLab) using Cu-Kα radiation. The particle morphologies of the synthesized $Na_2Ti_3O_7$/C powders were observed by a field emission scanning electron microscope (FE-SEM, Hitachi, SU8000).

The $Na_2Ti_3O_7$/C electrodes were fabricated by mixing $Na_2Ti_3O_7$/C (80 wt%), acetylene black (15 wt%), and polyamide-imide (5 wt%) in *N*-methyl-2-pyrrolidone (NMP) solution to form a uniform slurry, which was then coated onto an Al foil. The coated $Na_2Ti_3O_7$/C electrodes were dried in vacuum at 393 K overnight before being transferred into an Ar-filled glove box. The mass loading of the $Na_2Ti_3O_7$ on the Al foil was 1.8-2.3 mg cm^{-2}. Charge-discharge testing was performed using R2032-type coin cells with sodium foils as the counter electrodes and glass fiber filters (Whatman, GF-A, 260 mm) as the separators.

Na[FSA]-[C_3C_1pyrr][FSA] ionic liquid with a molar ratio of 2:8 was adopted as the electrolyte [28]. The $Na_2Ti_3O_7$/C electrodes and separators were vacuum-impregnated with Na[FSA]-[C_3C_1pyrr][FSA] ionic liquid at 333 K before assembling the coin cells in an Ar-filled glove box. Charge-discharge tests were conducted at constant current rates of 20–2000 mA g^{-1} in the voltage range 0.01–2.5 V. The cycle performance was evaluated at constant current rates of 20, 100, 200, and 500 mA g^{-1}. Electrochemical impedance measurements were performed before and after the charge-discharge cycles in the frequency range of 200 kHz to 100 mHz with an AC voltage signal of 10 mV. All electrochemical measurements were performed at 363 K. After the charge-discharge tests, the $Na_2Ti_3O_7$/C electrodes were removed from the testing cells and washed with anhydrous tetrahydrofuran (THF; Wako Pure Chemicals) in an Ar-filled glove box to remove the electrolyte. The crystal structure and morphology of the $Na_2Ti_3O_7$/C electrodes were investigated by XRD and SEM, where the electrodes were sealed in an airtight sample holder to avoid air exposure.

3. Results and discussion

The XRD patterns of the synthesized $Na_2Ti_3O_7$ and $Na_2Ti_3O_7$/C powders are shown in Fig. 1A. All the diffraction peaks can be indexed to the $Na_2Ti_3O_7$ phase (JCPDS file No. 00-031-1329), and no impurity phase was observed, indicating that carbon coating does not alter the original $Na_2Ti_3O_7$ crystal structure. The carbon content in the $Na_2Ti_3O_7$/C powders was determined to be approximately 5.0 wt% by a CHN analyzer. Fig. 1B shows the SEM image of the $Na_2Ti_3O_7$/C powders. The $Na_2Ti_3O_7$/C powders consist of small particles in the size range 100–500 nm and big plate-like particles in the size range 1–2 μm.

Fig. 2A shows the cyclic voltammograms of the $Na_2Ti_3O_7$/C electrode for the initial three cycles at a scan rate of 0.05 mV s^{-1} in the voltage range 0.0–2.5 V. In the first cycle, the reduction (Na insertion) process exhibits three peaks: a broad peak at around 1.2 V, a sharp peak at 0.1 V, and a smaller sharp peak at 0.0 V. Upon subsequent cycling, the peak at around 1.2 V vanishes completely, while the peak at 0.1 V shifts to 0.15 V, and the one at 0.0 V remains unaltered. The reduction peak at around 1.2 V can be attributed to some side-reactions including electrolyte reduction and the formation of the solid-electrolyte interphase (SEI) [20, 22]. The reduction peak at around 0.1 V is attributable to the insertion of Na ions into $Na_2Ti_3O_7$/C. The small reduction peak at 0.0 V is attributed to the insertion of Na ions into carbon black [20]. The first oxidation (Na extraction) process consists of two sharp peaks: a small peak at 0.08 V and a large peak at 0.41 V, which do not change with cycling. The oxidation peak at 0.08 V can be related to the extraction of Na ions from carbon black, while the oxidation peak at 0.41 V is attributed to the extraction of Na ions from $Na_2Ti_3O_7$/C.

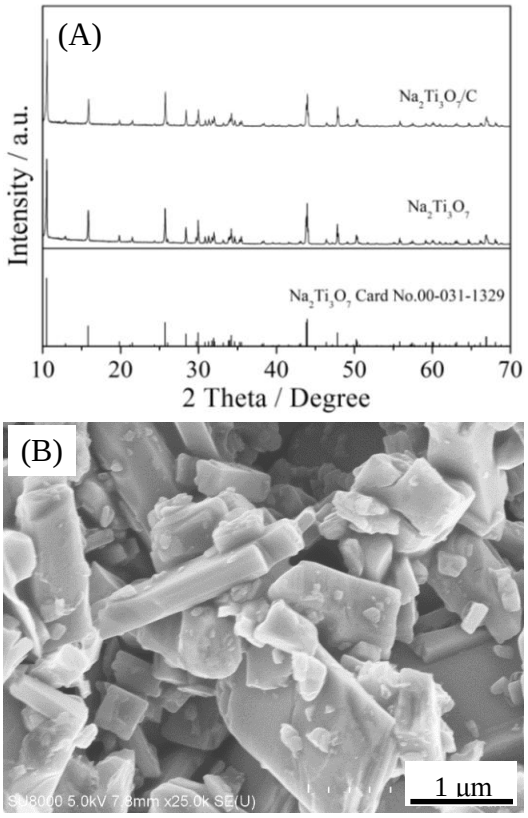

Fig. 1 (A) XRD pattern and (B) SEM image of the synthesized $Na_2Ti_3O_7$/C powders.

Fig. 2B presents the charge-discharge curves of the $Na_2Ti_3O_7$/C electrode at a current rate of 20 mA $(g\text{-}Na_2Ti_3O_7/C)^{-1}$ in the voltage range 0.01–2.5 V. In the first charge process, there are two distinct plateaus at about 1.3 and 0.15 V, while the discharge process shows a plateau at around 0.4 V. These results are in agreement with the observations in the CV curves (Fig. 2A). Upon subsequent cycles, the voltage plateau at about 1.3 V in the charge process, which is related to the side-reactions, vanishes completely, while the plateaus at about 0.15 V in the charge process and 0.4 V in the discharge process remain unchanged. The $Na_2Ti_3O_7$/C electrode shows a large initial charge capacity of 425 mAh $(g\text{-}Na_2Ti_3O_7/C)^{-1}$. However, the first discharge capacity is 215 mAh $(g\text{-}Na_2Ti_3O_7/C)^{-1}$, which implies a large irreversible capacity of 210 mAh g^{-1} and a low coulombic efficiency of 51%. The large irreversible capacity may be attributed to the side reactions including electrolyte reduction and SEI formation.

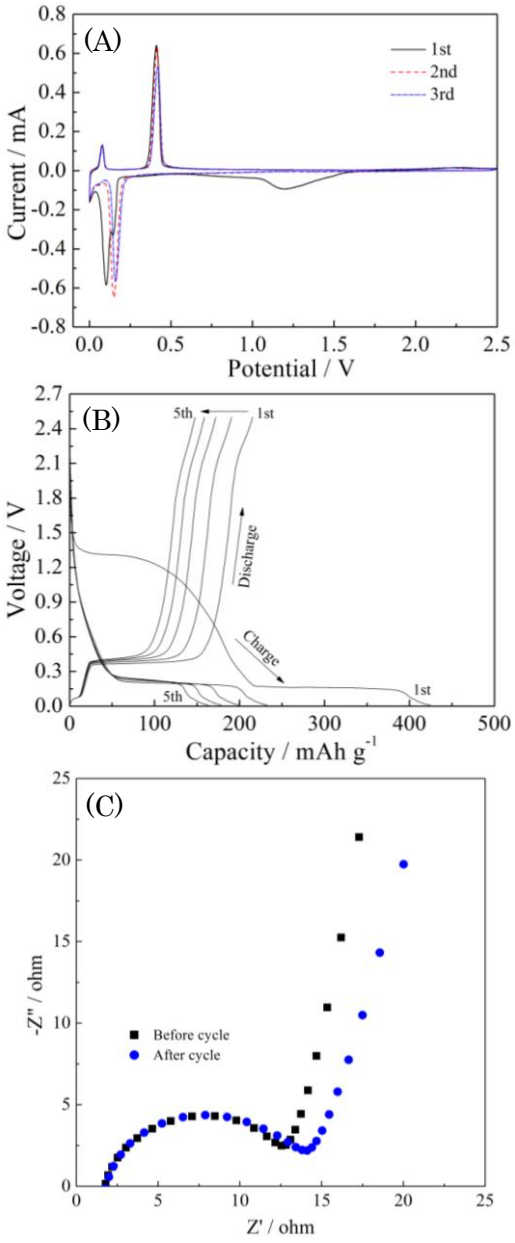

Fig. 2 (A) Cyclic voltammograms at a scan rate of 0.05 mV s^{-1}, (B) Charge-discharge curves at current rate of 20 mA g^{-1}, and (C) Nyquist plots obtained before and after five charge-discharge cycles for the $Na_2Ti_3O_7$/C electrode.

The initial reversible discharge capacity (215 mAh g^{-1}) of the $Na_2Ti_3O_7$/C electrode in the ionic liquid electrolyte is higher than those reported for the $Na_2Ti_3O_7$ electrodes in organic electrolytes: 178 mAh g^{-1} for ball-milled $Na_2Ti_3O_7$ powders [20], 185 mAh g^{-1} for $Na_2Ti_3O_7$ rods [21], ~180 mAh g^{-1} for $Na_2Ti_3O_7$ nanotubes [37], 188 mAh g^{-1} for $Na_2Ti_3O_7$ powders [22], ~205 mAh g^{-1} for $Na_2Ti_3O_7$ powders synthesized by the spray-drying method [23], and 177 mAh g^{-1} for $Na_2Ti_3O_7$/C powders [24]. A high reversible capacity indicates that there are more Na ions reversibly inserted into the $Na_2Ti_3O_7$/C electrode in ionic liquid electrolyte. Due to

the open layered framework, the $Na_2Ti_3O_7$ electrode can store a maximum of 3.5 Na ions per formula unit in the interlayer space [38, 39]. In general, for $Na_2Ti_3O_7$ electrodes in organic electrolyte, 2 Na ions per formula unit can be reversibly inserted into $Na_2Ti_3O_7$ to form $Na_4Ti_3O_7$ [19, 20, 24]. The theoretical capacities corresponding to the insertion of 2, 2.5, 3, and 3.5 Na ions per formula unit are 178, 222, 267, and 310 mAh g^{-1}, respectively. In this study, the reversible capacity is 215 mAh g^{-1}, which suggests that there are ~2.5 Na ions per formula unit reversibly inserted into $Na_2Ti_3O_7$.

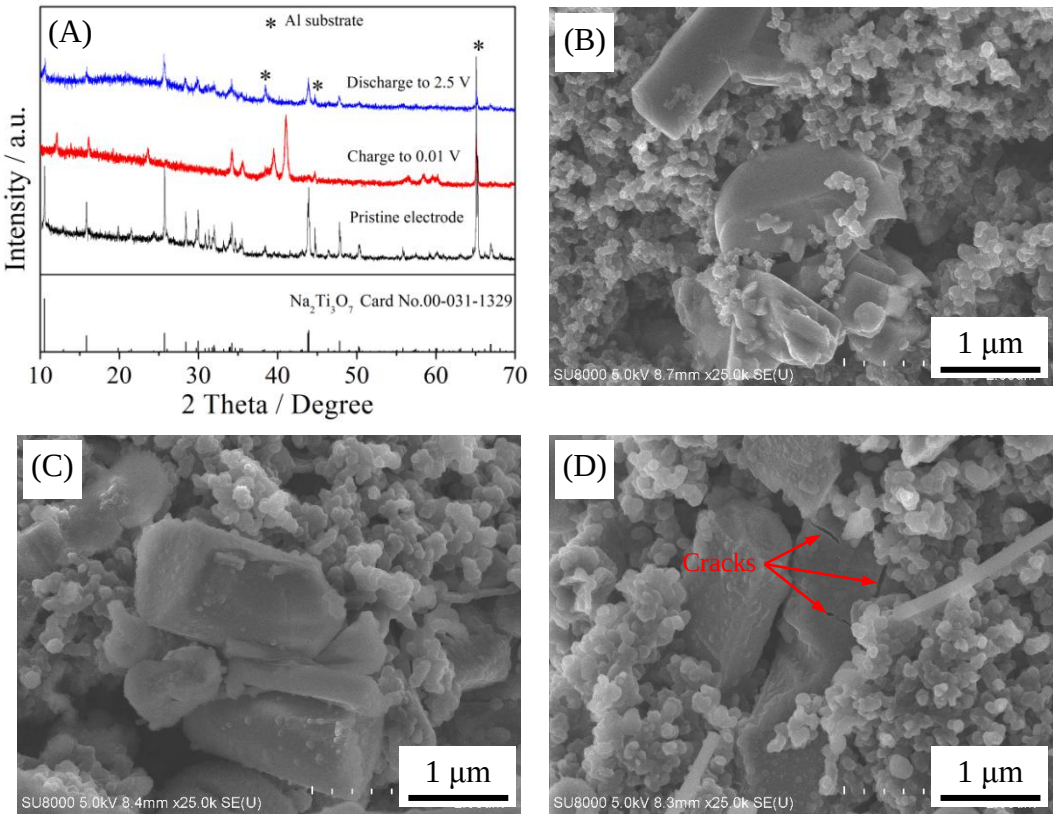

Fig. 3 (A) Ex-situ XRD patterns and (B-D) SEM images for the $Na_2Ti_3O_7$/C electrodes at different charge/discharge states: (B) pristine electrode, (C) charged to 0.01 V, and (D) discharged to 2.5 V.

Fig. 3A shows the XRD patterns of the $Na_2Ti_3O_7$/C electrodes at different charge-discharge states. When the $Na_2Ti_3O_7$/C electrode is charged to 0.01 V, the $Na_2Ti_3O_7$ crystal phase disappears and a new crystal phase appears. The pattern for the new crystal phase is characterized by the peaks at 2θ values of 12.1, 16.2, 23.7, 34.2, 35.6, 39.5, and 41.1° that correspond well with that reported in the literature [19], where the crystal phase formed is suggested to be $Na_4Ti_3O_7$. According to the theoretical and measured capacities, however, ~2.8 Na ions per formula unit are suggested to be inserted into the $Na_2Ti_3O_7$/C electrode to form $Na_{4.8}Ti_3O_7$. This is because the $Na_2Ti_3O_7$ electrode shows a higher capacity in ionic

liquid electrolyte at 363 K than in organic electrolytes at room temperature, which indicates a higher number of Na ions inserted into the electrode. When the $Na_2Ti_3O_7$/C electrode is discharged to 2.5 V, the new crystal phase disappears and the $Na_2Ti_3O_7$ crystal phase reappears. Thus, the Na ions can be reversibly inserted/extracted into/from the $Na_2Ti_3O_7$/C electrode. Considering the observed discharge capacity, ~2.5 Na ions per formula unit are extracted from the charged $Na_2Ti_3O_7$/C electrode, leaving behind ~0.3 Na ions during the discharge process.

Fig. 2B also shows that the capacity decreases rapidly with increasing cycle number. The capacity retention after 5 cycles is 69%, which is lower than that (>75%) in conventional organic electrolytes [20-22]. To investigate the reason for this decrease in capacity, impedance measurements were conducted before and after charge-discharge testing. Fig. 2C shows the Nyquist plots of the $Na_2Ti_3O_7$/C electrode before and after 5 charge-discharge cycles. The high frequency limit is the electrolyte resistance, which is unchanged after 5 charge-discharge cycles. The semicircle at the middle frequency corresponds to the charge-transfer process at the electrode/electrolyte interface. From Fig. 2C, it can be seen that the change in the charge-transfer resistance is not obvious before and after 5 charge-discharge cycles. This implies that the internal resistance is not the main reason for the degradation of the capacity. $Na_2Ti_3O_7$ usually suffers from sluggish Na insertion/extraction kinetics due to the insulating nature of the lattice associated with a large band gap of 3.7 eV [39, 40]. The capacity degradation with cycles might be due to the mechanical strain upon Na insertion as well as the irreversible insertion of some Na ions [24, 40, 41].

Fig. 3B-D shows the SEM images of the $Na_2Ti_3O_7$/C electrodes at different charge-discharge states. In the pristine electrode (Fig. 3B), the observed large and small particles are those of $Na_2Ti_3O_7$/C and acetylene black, respectively. When the electrode is charged to 0.01 V, there is no obvious change observed in the $Na_2Ti_3O_7$/C particles, except for the formation of some small particles on the surface (Fig. 3C). Rousse et al. reported that the unit cell volume of $Na_2Ti_3O_7$ increases by 5% when Na ions are inserted into it to form $Na_4Ti_3O_7$ [42]. Thus, the volume of the electrode should increase upon Na insertion, and when the electrode is discharged to 2.5 V, the volume of $Na_2Ti_3O_7$/C particles decreases due to Na extraction. The expansion and contraction of the $Na_2Ti_3O_7$/C particles would result in the formation of cracks, as observed in the discharged electrode (Fig. 3D). Thus, the formation of cracks due to Na insertion/extraction is also responsible for the capacity degradation.

The rate capability of the $Na_2Ti_3O_7$/C electrode was also measured at current rates of 20–2000 mA g^{-1} in the voltage range 0.01–2.5 V (Fig. 4A). The discharge capacity decreases upon increasing the current rate. At current rates of less than 100 mA g^{-1}, the discharge capacity decreases quickly from 219 mAh g^{-1} at 20 mA g^{-1} to 119 mAh g^{-1} at 50 mA g^{-1}. At current rates higher than 100 mA g^{-1}, the discharge capacity decreases slowly with an increase

in the current rate. A similar phenomenon was also reported for the $Na_2Ti_3O_7$ electrodes in organic electrolytes [20, 22]. The discharge capacities are 80 and 57 mAh g^{-1} at current rates of 500 and 2000 mA g^{-1}, respectively. The rate capability in ionic liquid electrolyte is comparable to that in organic electrolytes. The low capacity at high current rate results from the capacity decay at low current rates. When the current rate is returned to 20 mA g^{-1} after the rate testing, the electrode only shows a discharge capacity of 102 mAh g^{-1}, indicating that the capacity reduction at high current rate is ca. 117 mAh g^{-1} due to the capacity decay. The coulombic efficiency gradually increases with increasing current rate, and at high current rates becomes > 99%.

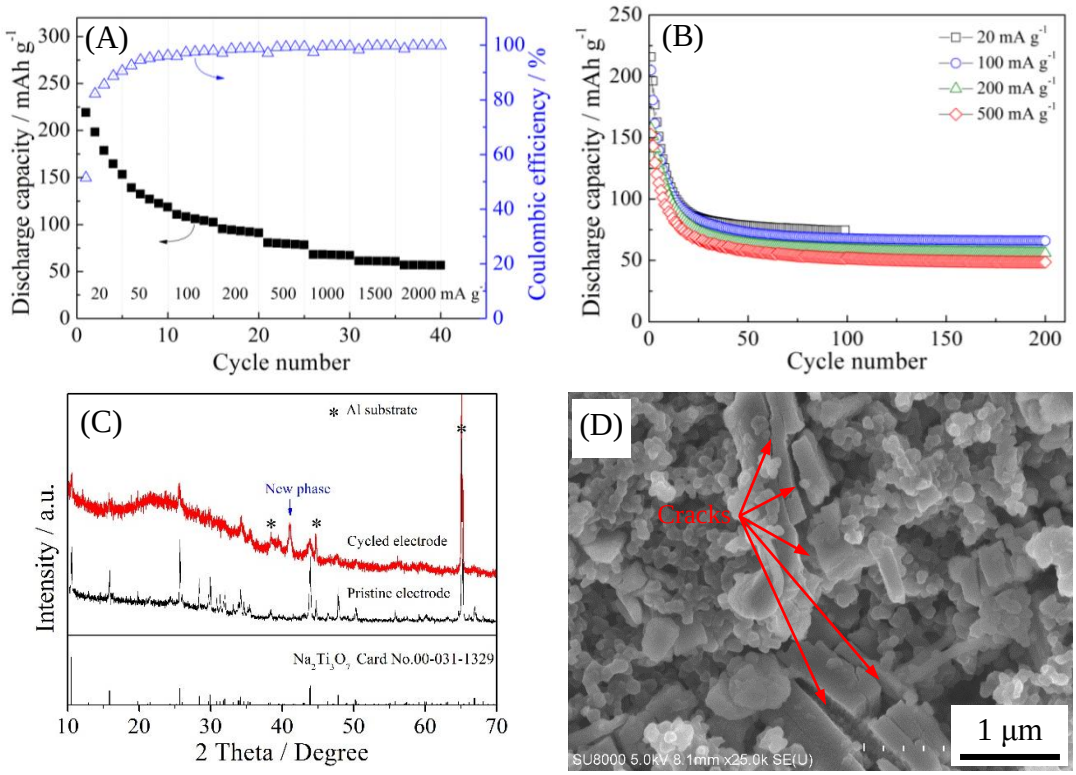

Fig. 4 (A) Rate capability and (B) Cycle performance of the $Na_2Ti_3O_7$/C electrode, (C) XRD pattern and (D) SEM image of the $Na_2Ti_3O_7$/C electrode after charging/discharging at 100 mA g^{-1} for 25 cycles.

The cycle performance of the $Na_2Ti_3O_7$/C electrode is displayed in Fig. 4B for 200 cycles at current rates of 20, 100, 200, and 500 mA g^{-1}. It can be noted that the discharge capacity declines rapidly before 25 cycles at all the current rates, and is almost unchanged in the subsequent cycles. In the first cycle, the discharge capacities are 216, 205, 157, and 153 mAh g^{-1} at current rates of 20, 100, 200, and 500 mA g^{-1}, respectively. The discharge capacity at 500 mA g^{-1} is higher than that shown in Fig. 4A, which indicates the effect of capacity decay

on rate capability. After 50 cycles, the discharge capacities are 78.5, 73.1, 63.6, and 58.0 mAh g^{-1} at current rates of 20, 100, 200, and 500 mA g^{-1}, respectively. The low discharge capacity results from the quick capacity decay before 25 cycles. The quick capacity decay may be attributed to the irreversible insertion of some Na ions [21, 40] and the formation of cracks due to Na insertion/extraction (as shown in Fig. 3D). Fig. 4C shows the XRD pattern of the $Na_2Ti_3O_7$/C electrode after charging/discharging at 100 mA g^{-1} for 25 cycles. A new crystal phase found in the cycled electrode is similar with the one observed in Fig. 3A for the charged electrode, indicating that some inserted Na ions have not been extracted. Fig. 4D shows the SEM image of the same cycled electrode. Many cracks are observed for the $Na_2Ti_3O_7$/C particles and some $Na_2Ti_3O_7$/C particles have been pulverized. Thus, the formation of cracks and the pulverization of particles result in both the irreversible insertion of Na ions and the quick capacity fading. The conductivity and stability of this material can be improved by using nanostructured $Na_2Ti_3O_7$. Some reports [39, 40, 43, 44] have shown that the cycle performance of $Na_2Ti_3O_7$ electrodes in organic electrolytes have been improved by using nanostructured $Na_2Ti_3O_7$ like nanotubes, nanosheets, and nanoarrays. Therefore, nanostructured $Na_2Ti_3O_7$ electrodes are expected to show good rate capability and cycle performance in ionic liquid electrolyte.

4. Conclusions

$Na_2Ti_3O_7$/C powders were synthesized and their electrochemical performance was evaluated in Na[FSA]-[C_3C_1pyrr][FSA] ionic liquid electrolyte at 363 K. The $Na_2Ti_3O_7$/C electrode showed a high discharge capacity of 215 mAh g^{-1} at a current rate of 20 mA g^{-1} in the voltage range 0.01–2.5 V. The $Na_2Ti_3O_7$/C electrode also showed a relatively good rate capability. However, due to the degradation behavior, the $Na_2Ti_3O_7$/C electrode showed poor cycle performance. The results show that $Na_2Ti_3O_7$/C is a promising negative electrode material because of its high capacity, but more efforts are needed to improve its rate capability and cycle performance.

Acknowledgements

This study was partly supported by the Advanced Low Carbon Technology Research and Development Program (ALCA, No. 3428) of the Japan Science and Technology Agency (JST), and the Elements Strategy for Catalysts and Batteries (ESICB) program of the Japanese Ministry of Education, Culture, Sports, Science and Technology (MEXT).

References

[1] M.D. Slater, D. Kim, E. Lee, C.S. Johnson, Adv. Funct. Mater., 23 (2013) 947-958.
[2] B.L. Ellis, L.F. Nazar, Curr. Opin. Solid State Mater. Sci., 16 (2012) 168-177.

[3] N. Yabuuchi, M. Kajiyama, J. Iwatate, H. Nishikawa, S. Hitomi, R. Okuyama, R. Usui, Y. Yamada, S. Komaba, Nat. Mater., 11 (2012) 512-517.
[4] V. Palomares, P. Serras, I. Villaluenga, K.B. Hueso, J. Carretero-Gonzalez, T. Rojo, Energy Environ. Sci., 5 (2012) 5884-5901.
[5] J.S. Thorne, R.A. Dunlap, M.N. Obrovac, J. Electrochem. Soc., 160 (2013) A361-A367.
[6] J.M. Clark, P. Barpanda, A. Yamada, M.S. Islam, J. Mater. Chem. A, 2 (2014) 11807-11812.
[7] Z.L. Jian, W.Z. Han, X. Lu, H.X. Yang, Y.S. Hu, J. Zhou, Z.B. Zhou, J.Q. Li, W. Chen, D.F. Chen, L.Q. Chen, Adv. Energy Mater., 3 (2013) 156-160.
[8] J. Billaud, R.J. Clement, A.R. Armstrong, J. Canales-Vazquez, P. Rozier, C.P. Grey, P.G. Bruce, J. Am. Chem. Soc., 136 (2014) 17243-17248.
[9] L.P. Wang, L.H. Yu, X. Wang, M. Srinivasan, Z.C.J. Xu, J. Mater. Chem. A, 3 (2015) 9353-9378.
[10] J.W. Wang, X.H. Liu, S.X. Mao, J.Y. Huang, Nano Lett., 12 (2012) 5897-5902.
[11] Y.H. Xu, Y.J. Zhu, Y.H. Liu, C.S. Wang, Adv. Energy Mater., 3 (2013) 128-133.
[12] Z. Li, J. Ding, D. Mitlin, Acc. Chem. Res., 48 (2015) 1657-1665.
[13] S. Komaba, W. Murata, T. Ishikawa, N. Yabuuchi, T. Ozeki, T. Nakayama, A. Ogata, K. Gotoh, K. Fujiwara, Adv. Funct. Mater., 21 (2011) 3859-3867.
[14] A. Ponrouch, A.R. Goni, M.R. Palacin, Electrochem. Commun., 27 (2013) 85-88.
[15] K.-l. Hong, L. Qie, R. Zeng, Z.-q. Yi, W. Zhang, D. Wang, W. Yin, C. Wu, Q.-j. Fan, W.-x. Zhang, Y.-h. Huang, J. Mater. Chem. A, 2 (2014) 12733-12738.
[16] Y. Xu, E.M. Lotfabad, H. Wang, B. Farbod, Z. Xu, A. Kohandehghan, D. Mitlin, Chem. Commun., 49 (2013) 8973-8975.
[17] L. Wu, D. Buchholz, D. Bresser, L. Gomes Chagas, S. Passerini, J. Power Sources, 251 (2014) 379-385.
[18] K.T. Kim, G. Ali, K.Y. Chung, C.S. Yoon, H. Yashiro, Y.K. Sun, J. Lu, K. Amine, S.T. Myung, Nano Lett., 14 (2014) 416-422.
[19] P. Senguttuvan, G. Rousse, V. Seznec, J.-M. Tarascon, M.R. Palacín, Chem. Mater., 23 (2011) 4109-4111.
[20] A. Rudola, K. Saravanan, C.W. Mason, P. Balaya, J. Mater. Chem. A, 1 (2013) 2653.
[21] W. Wang, C.J. Yu, Y.J. Liu, J.G. Hou, H.M. Zhu, S.Q. Jiao, RSC Adv., 3 (2013) 1041-1044.
[22] H. Pan, X. Lu, X. Yu, Y.-S. Hu, H. Li, X.-Q. Yang, L. Chen, Adv. Energy Mater., 3 (2013) 1186-1194.
[23] W. Zou, J.W. Li, Q.J. Deng, J. Xue, X.Y. Dai, A.J. Zhou, J.Z. Li, Solid State Ion., 262 (2014) 192-196.
[24] J. Xu, C.Z. Ma, M. Balasubramanian, Y.S. Meng, Chem. Commun., 50 (2014) 12564-12567.

[25] T. Nohira, T. Ishibashi, R. Hagiwara, J. Power Sources, 205 (2012) 506-509.
[26] A. Fukunaga, T. Nohira, Y. Kozawa, R. Hagiwara, S. Sakai, K. Nitta, S. Inazawa, J. Power Sources, 209 (2012) 52-56.
[27] T. Yamamoto, T. Nohira, R. Hagiwara, A. Fukunaga, S. Sakai, K. Nitta, S. Inazawa, Electrochim. Acta, 135 (2014) 60-67.
[28] C.S. Ding, T. Nohira, K. Kuroda, R. Hagiwara, A. Fukunaga, S. Sakai, K. Nitta, S. Inazawa, J. Power Sources, 238 (2013) 296-300.
[29] C.S. Ding, T. Nohira, R. Hagiwara, J. Mater. Chem. A, 3 (2015) 20767-20771.
[30] C. Ding, T. Nohira, R. Hagiwara, A. Fukunaga, S. Sakai, K. Nitta, Electrochim. Acta, 176 (2015) 344-349.
[31] C.H. Wang, Y.W. Yeh, N. Wongittharom, Y.C. Wang, C.J. Tseng, S.W. Lee, W.S. Chang, J.K. Chang, J. Power Sources, 274 (2015) 1016-1023.
[32] N. Wongittharom, C.H. Wang, Y.C. Wang, C.H. Yang, J.K. Chang, ACS Appl. Mater. Inter., 6 (2014) 17564-17570.
[33] C.H. Wang, C.H. Yang, J.K. Chang, Chem. Commun., 52 (2016) 10890-10893.
[34] I. Hasa, S. Passerini, J. Hassoun, J. Power Sources, 303 (2016) 203-207.
[35] C. Ding, T. Nohira, R. Hagiwara, K. Matsumoto, Y. Okamoto, A. Fukunaga, S. Sakai, K. Nitta, S. Inazawa, J. Power Sources, 269 (2014) 124-128.
[36] C.Y. Chen, K. Matsumoto, T. Nohira, C.S. Ding, T. Yamamoto, R. Hagiwara, Electrochim. Acta, 133 (2014) 583-588.
[37] W. Wang, C. Yu, Z. Lin, J. Hou, H. Zhu, S. Jiao, Nanoscale, 5 (2013) 594-599.
[38] Y.P. Zhang, L. Guo, S.H. Yang, Chem. Commun., 50 (2014) 14029-14032.
[39] S.D. Fu, J.F. Ni, Y. Xu, Q. Zhang, L. Li, Nano Lett., 16 (2016) 4544-4551.
[40] J.F. Ni, S.D. Fu, C. Wu, Y. Zhao, J. Maier, Y. Yu, L. Li, Adv. Energy Mater., 6 (2016).
[41] M.A. Munoz-Marquez, M. Zarrabeitia, E. Castillo-Martinez, A. Eguia-Barrio, T. Rojo, M. Casas-Cabanas, ACS Appl. Mater. Inter., 7 (2015) 7801-7808.
[42] G. Rousse, M.E. Arroyo-de Domablo, P. Senguttuvan, A. Ponrouch, J.M. Tarascon, M.R. Palacin, Chem. Mater., 25 (2013) 4946-4956.
[43] H.S. Li, L.L. Peng, Y. Zhu, D.H. Chen, X.G. Zhang, G.H. Yu, Energy Environ. Sci., 9 (2016) 3399-3405.
[44] S.Y. Dong, L.F. Shen, H.S. Li, G. Pang, H. Dou, X.G. Zhang, Adv. Funct. Mater., 26 (2016) 3703-3710.